PB88-102736

Microscopic Evaluation of Efficiency Theory for Electrostatic Precipitators

Research Triangle Inst.
Research Triangle Park, NC

Prepared for

Environmental Protection Agency
Research Triangle Park, NC

Sep 87

U.S. Department of Commerce
National Technical Information Service
NTIS

PB88-102736

EPA/600/D-87/246
September 1987

MICROSCOPIC EVALUATION OF EFFICIENCY THEORY FOR ELECTROSTATIC PRECIPITATORS

By

Toshiaki Yamamoto
Research Triangle Institute
Research Triangle Park, NC 27709

EPA Project Officer
Leslie E. Sparks

CR808936

AIR AND ENERGY ENGINEERING RESEARCH LABORATORY
OFFICE OF RESEARCH AND DEVELOPMENT
U.S. ENVIRONMENTAL PROTECTION AGENCY
RESEARCH TRIANGLE PARK, NC 27711

REPRODUCED BY
U.S. DEPARTMENT OF COMMERCE
NATIONAL TECHNICAL
INFORMATION SERVICE
SPRINGFIELD, VA 22161

TECHNICAL REPORT DATA
(Please read Instructions on the reverse before completing)

1. REPORT NO. EPA/600/D-87/246	2.
3. RECIPIENT'S ACCESSION NO. PB88-102736	
4. TITLE AND SUBTITLE Microscopic Evaluation of Efficiency Theory for Electrostatic Precipitators	5. REPORT DATE September 1987
	6. PERFORMING ORGANIZATION CODE
7. AUTHOR(S) Toshiaki Yamamoto	8. PERFORMING ORGANIZATION REPORT NO.
9. PERFORMING ORGANIZATION NAME AND ADDRESS Research Triangle Institute P.O. Box 12194 Research Triangle Park, North Carolina 27709	10. PROGRAM ELEMENT NO.
	11. CONTRACT/GRANT NO. Cooperative Agreement CR808936
12. SPONSORING AGENCY NAME AND ADDRESS EPA, Office of Research and Development Air and Energy Engineering Research Laboratory Research Triangle Park, NC 27711	13. TYPE OF REPORT AND PERIOD COVERED Published Paper; 12/84
	14. SPONSORING AGENCY CODE EPA/600/13

15. SUPPLEMENTARY NOTES AEERL project officer is Leslie E. Sparks, Mail Drop 61, 919/541-2458.

16. ABSTRACT The paper discusses a microscopic evaluation of efficiency theory for electrostatic precipitators. A wire-plate configuration is selected, and the position dependence of migration velocity, concentration profiles, and fractional-collection efficiency is discussed. Several efficiency theories, including non-Deutchian phenomena, have appeared over the years. Among all existing theories, the effective migration is the quantity in dispute and not the theoretical migration velocity. The particle-migration velocity cannot be a single number but is rather a function of position. The local migration velocity is essential to calculate the concentration profile. Therefore, the theoretical treatment of particle motion in the electrohydrodynamic field is a necessary step in understanding the microscopic precipitation process and efficiency theory.

17. KEY WORDS AND DOCUMENT ANALYSIS

a. DESCRIPTORS		b. IDENTIFIERS/OPEN ENDED TERMS	c. COSATI Field/Group	
Pollution	Efficiency	Pollution Control	13B	
Electrostatic Precipitators	Particles	Stationary Sources		
	Electrostatics	Effective Migration	13I	20C
Electrohydrodynamics	Mathematical Models	Concentration Profiles		12A
		Fractional-collection Efficiency	20I	
Collection			14G	

18. DISTRIBUTION STATEMENT Release to Public	19. SECURITY CLASS (This Report) Unclassified	21. NO. OF PAGES 13
	20. SECURITY CLASS (This page) Unclassified	22. PRICE A02 9.95

EPA Form 2220-1 (9-73)

NOTICE

This document has been reviewed in accordance with U.S. Environmental Protection Agency policy and approved for publication. Mention of trade names or commercial products does not constitute endorsement or recommendation for use.

EPA/600/D-87/246
September 1987

MICROSCOPIC EVALUATION OF EFFICIENCY THEORY FOR ELECTROSTATIC PRECIPITATORS

Toshiaki Yamamoto

Research Triangle Institute
P.O. Box 12194
Research Triangle Park, NC 27709

ABSTRACT

Several efficiency theories, including non-Deutschian phenomena, have appeared over the years. Among all existing theories, the effective migration is the quantity in dispute and not the theoretical migration velocity. The particle-migration velocity cannot be a single number but is rather a function of position. The local migration velocity is essential to calculate the concentration profile. Therefore, the theoretical treatment of particle motion in the electrohydrodynamic (EHD) field is a necessary step in understanding the microscopic precipitation process and efficiency theory.

In this paper the wire-plate configuration is selected, and the position dependence of migration velocity, concentration profiles, and fractional-collection efficiency are discussed. Microscopic evaluation of efficiency theory are discussed toward a unified efficiency theory.

INTRODUCTION

In the process of particle collection in an electrostatic precipitator, the charged particles are transported to the collector walls by the combined influences of the Coulomb force due to the electrostatic field and of particle interaction with the flowing gas.

Most operating precipitators use negative corona which occurs in finite tufts along the length of the corona wire, producing field variations in this dimension. Therefore, the fluid field coupled with the secondary flow caused by the negative corona becomes nonuniform and three dimensional. The flow interaction is generally too complicated to isolate the effects of individual parameters. However, positive corona is produced uniformly along the corona wire; thus, field variations in this direction are minimized, and the flow field will be two dimensional.

The pictures of particle motion for low-turbulent intensity ($T \approx 0.9\%$) [1] and for high-turbulent intensity [2] have suggested that the paths of the small particles follow very closely to the calculated electrohydrodynamic (EHD) path. This implies that the particle transport by the EHD force is more significant than the transport due to the aerodynamic source of turbulence. Shaughnessy et al. [3] have made a similar observation. Assuming that there are no large-scale eddies and that there is a low level of turbulence at the duct entrance conditions, the laminar flow assumption is adequate to describe the flow field. Therefore, turbulent diffusion is neglected in the present simulation.

Among usual efficiency theories, an effective migration velocity is a single number, but the quantity under consideration here is not the theoretical migration velocity. The improved theoretical treatment of the particle motion in the EHD field is a necessary step in understanding the microscopic precipitation process and efficiency theory. In this paper the local migration velocity, concentration profiles, and fraction collection efficiency are discussed, and the implications of the results to precipitator performance are discussed.

MATHEMATICAL MODEL

Figure 1 shows the physical arrangement for a mathematical model for precipitation-theory description. The work consists of four steps. The first step is an investigation of the electrostatic field and the space-charge-density distribution. This analysis is independent of any flow field, provided the primary flow velocity is much smaller than the ion velocity and will determine the driving force for the ionic wind.

For the boundary conditions, a uniform flow distribution is assumed at the inlet, whereas the outlet-boundary condition is that the streamlines are orthogonal to the outlet boundary without fixing the velocity distribution or its magnitude. The nonslip condition is applied along the plate surface. The symmetry condition is used along the centerline of the channel.

The calculated numerical results demonstrated close agreement with the experiment [5]. Also, Leonard, Mitchner, and Self [6, 7] have observed similar EHD flow patterns.

3. The Equation of Motion for the Particles

The equation of motion of a spherical particle in the EHD field is expressed as:

$$m \frac{d\vec{V}_p}{dt} = q \vec{E} - 6\pi \mu a f_1 (\vec{V}_p - \vec{V}_f) , \quad (5)$$

where m is the mass of the particle; $\vec{V}_p$ and $\vec{V}_f$ are the velocity vector of the particle and the fluid, respectively; a is the radius of the particle; f_1 is a correction factor to the Stokes' drag based on the particle Reynolds number; q is the particle charge; and μ is the viscosity coefficient. The motion of a particle can be calculated by integrating the equations. The motion of the particles is nondimensionalized by using the primary velocity, U_o, average field strength, $E_o = V_o/d$, wire-plate distance, d, and m:

$$\frac{d\vec{V}^*_p}{dt^*} + \zeta \vec{V}^*_p = \zeta \vec{V}^*_f + \xi \vec{E}^* , \quad (6)$$

where:

$$\vec{V}^*_p = \vec{V}_p/U_o , \quad \vec{E}^* = \frac{\vec{E}}{E_o} , \quad t^* = t/(d/U_o) ,$$

$$\zeta = 6\pi \mu a U_o f_1/(m U_o^2/d), \quad \xi = q E_o/(m U_o^2/d). \quad (7)$$

As seen in Equation (7), ζ represents the effect of viscous drag force. Typical precipitator operation falls in the range of $\zeta >> 1$. This implies that the viscous force is considerably greater than the inertia force, which corresponds to Stokes' flow hypothesis. On the other hand, ξ represents the effect of electrostatic force.

The motion of particles is evaluated by two dimensionless parameters. The first dimensionless parameter is the EHD number, N_{EHD}, which is a ratio of the secondary flow to the primary flow, thus defined as:

$$N_{EHD} = \left(\frac{J_o d}{K \rho}\right)^{1/2} /2U_o = \frac{U_e}{2U_o} , \quad (8)$$

where J_o is average current density at the plate, and U_e is defined as characteristic secondary-flow velocity. By using the N_{EHD}, ζ, and ξ, the new dimensionless parameter called the EHD charge number, N_{E-C}, is defined as:

$$N_{E-C} = 2N_{EHD} \frac{\xi}{\zeta} = \frac{qE_o}{6\pi n a U_o f_1} = \frac{De}{g} . \quad (9)$$

The N_{E-C} is a ratio of average electrostatic force to EHD drag force acting on the particle. The Deutsch number, $De = W_E A/Q$, used for Leonard et al. [8] is related to N_{E-C} g, where g is a geometric constant and defined by the ratio of plate width to plate-plate spacing. For the field-charging theory, large N_{E-C} corresponds to large particle diameter. The dimensionless force $\vec{Fe}^*$ can be written in terms of N_{E-C} and ξ as:

$$\vec{Fe}^* = \frac{\xi}{N_{E-C}} (\vec{V}^*_f + N_{E-C} \vec{E}^*) . \quad (10)$$

The value of N_{E-C} determines how closely the particle moves along the EHD streamlines. For $N_{E-C} >> 1$, the particle motion is effectively controlled by the electrostatic field, while for $N_{E-C} << 1$, the particle motion is dominated by the EHD streamlines. When $N_{E-C} \approx 1.0$, the particle motion is affected by both electrostatic and EHD fields. The typical value for N_{E-C} in the industrial precipitator is in the range of 0.01 to 0.5. Therefore, particles should follow the EHD-dominated pattern closely.

4. Particle Concentration Profile and Fractional Collection Efficiency

From the results of the particle-motion calculations, the concentration profiles can be determined for known concentration and velocity profiles at the inlet. At the same time, the fraction of the particle collected for the two-wire precipitator can also be calculated by using Lotus 1-2-3 on a TRS-80 Model 2000.

In order to determine the local concentration profile, the two adjacent particle pathlines, Ψ_i and Ψ_{i-1}, going through the points (i-1,j) and (i-1,j-1) are considered, as illustrated in Figure 2. Assuming that the particle concentration at the cell (i-1,j) is moved to the next cell and displaced to $\alpha_{i,j}\Delta y$ from the cell (i,j) and the concentration at the cell (i-1,j-1) is displaced by $\alpha_{i,j-1}\Delta y$ from the cell (i,j-1), then the particle concentration at the cell (i,j) can be expressed as:

$$C_{i,j} = C_{i-1,j}(1 - |\alpha_{i,j}|) + \alpha_{i,j-1} C_{i-1,j-1}$$

(for $\frac{\partial \Psi}{\partial x} \geq 0$) - $\alpha_{i,j+1} C_{i-1,j+1}$ (for $\frac{\partial \Psi}{\partial x} < 0$), (11)

where $\alpha_{i,j}$ is defined as the displacement coefficient ($|\alpha_{i,j}| \leq 1$), and determines the precipitation rate.

The boundary conditions used for the concentration profiles are:

$\alpha_{1,j}$ = 0 at the inlet;

$\alpha_{i,d}$ = $\alpha_{i,d-1}$ at the half cell of the wall (the slope of the particle pathline near the wall is unchanged);

$\alpha_{i,1}$ = $\alpha_{i,2}/2$ at the half cell of the centerline;

$C_{w,1}$ = 0 at the two wire locations; and

$C_{1,j}$ = C(y) at the inlet. (12)

All the values of $\alpha_{i,j\pm1}$ are actually interpolated as $\alpha_{i,j\pm1/2}$.

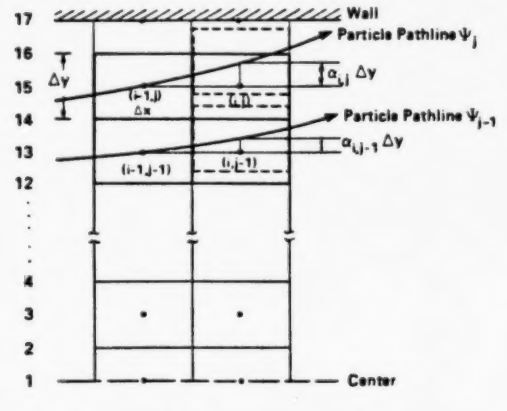

Figure 2. Control cell for the local concentration.

When the local concentration is calculated, the penetration is evaluated from the formula:

$$P_L = \int_0^d C_{L,j}\,dy \Big/ \int_0^d C_{1,j}\,dy \,. \qquad (13)$$

Overall penetration of a multisection precipitator can be obtained by repeating the calculations using the concentration and velocity profiles obtained at the outlet of the previous section as the inlet profile for the following section:

$$P = \prod_{j=1}^{N} P_{L,j} \,. \qquad (14)$$

It should be noted that Equation (5) applies only to a single class of particles so that Equation (13) refers to the fractional efficiency for a given size class. The overall mass efficiency must be obtained by appropriate integration over the prevailing distribution.

NUMERICAL RESULTS AND DISCUSSION

The numerical results for particle trajectories, concentration profiles, and fraction efficiency are obtained. Even though all parameters are attempted to express in terms of two dimensionless parameters, such as N_{EHD} and N_{E-C} in order to generalize the precipitation process, let us consider the following configuration which was used earlier in the laboratory.

The two-wire precipitator consists of a plate-to-plate distance of 6 cm, a wire-to-wire distance of 4.8 cm, and a wire diameter of 0.2 mm. Average field strength is E_o = 5.0 kV/cm, the current per unit length of corona wire is 1.1 mA/m, the charge on the particles acquires 73% of saturation charge, $q = 0.73\, q_s$ and precharged at the inlet, and f_1 is assumed to be 1. The particle density is assumed to be $\rho_s = 0.6\times10^3$ kg/m^3, temperature is 23°C, and pressure is 1 atm.

Figures 3 and 4 show the upper half section of the two-wire precipitator, which is divided into 17 sections at the inlet. The solid lines in Figures 3 and 4 represent the computed EHD streamlines: for U_o = 0.61 m/s and E_o = 5.0 kV/cm (or N_{EHD} = 2.89), and for U_o = 1.22 m/s and E_o = 5.0 kV/cm (or N_{EHD} = 1.38), respectively; while the particles starting at y = 2, 5, 8, 11, 14, and 16 are plotted during the same time intervals so that the local particle-migration velocity can be estimated from the figures. It should be noted that the vertical scale shown in all successive figures is stretched twice as much as the horizontal scale.

The EHD streamlines show that the fluid is gradually accelerated and deflected toward the center of the channel due to the circulatory cell generated directly above the corona wire as it approaches the corona. A large fraction of the cross-section area is blocked off by the circulatory cell, resulting in much faster gas flow in the center of the channel. After passing the corona wire, the streamline moves toward the plate with deceleration and repeats similarly for the successive wires. As the primary flow increases (or N_{EHD} decreases), the flow interaction becomes less significant as shown in Figures 3 and 4; and when the primary flow velocity exceeds 1.8 m/s (or $N_{EHD} < 0.6$), the flow interaction appears to be negligible.

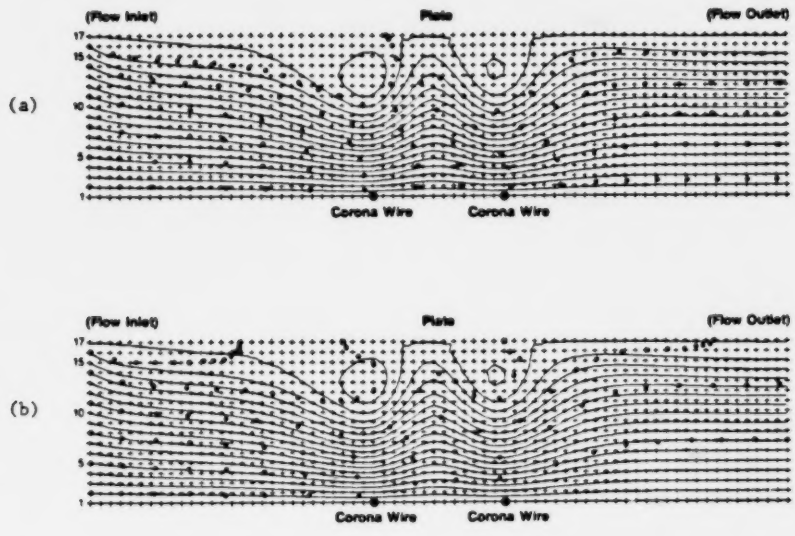

Figure 3. Particle trajectories for N_{EHD} = 2.96; U_o = 0.61 m/s; and E_o = 5.0 kV/cm. (a) 2a = 1 μm (N_{E-C} = 0.048), and (b) 2a = 5 μm (N_{E-C} = 0.24).

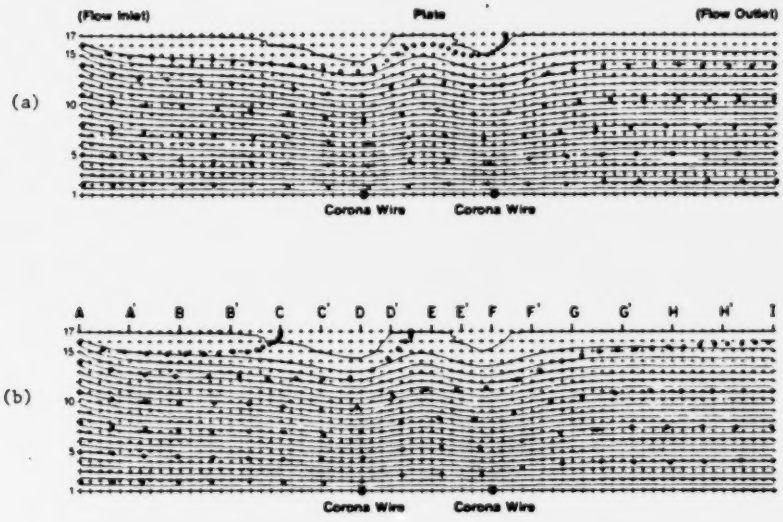

Figure 4. Particle trajectories for N_{EHD} = 1.34; U_o = 1.22 m/s; and E_o = 5.0 kV/cm. (a) 2a = 1 μm (N_{E-C} = 0.024), and (b) 2a = 5 μm (N_{E-C} = 0.12).

The particle trajectories for 1.0 μm and 5.0 μm in diameter are shown in Figures 3(a) and 3(b) when the primary velocity, U_o, is 0.61 m/s, which corresponds to $N_{E-C} = 0.048$ and $N_{E-C} = 0.24$. The particle trajectories for 1.0 μm and 5.0 μm in the higher primary velocity, $U_o = 1.22$ m/s (or $N_{E-C} = 0.24$ and $N_{E-C} = 0.120$) are shown in Figures 4(a) and 4(b). When the particle diameter increases (or N_{E-C} increases), the particles tend to depart from the EHD streamlines. The particles 1 μm in diameter move closer to EHD streamlines. Hence, the particle motion is largely controlled by the EHD force, resulting in a small fraction of the particles introduced near the wall being collected ($P \approx 0.825$ and 0.9 from Figures 3(a) and 4(a), respectively). On the other hand, as the particle size becomes larger (or N_{E-C} increases), it departs from the EHD streamlines, resulting in higher collection being achieved ($P \approx 0.375$ and 0.64 from Figures 3(b) and 4(b), respectively).

As can be seen from both figures, the particles initially move toward the corona wire, except for the particles in the vicinity of the collection plate. The local migration velocity is a negative quantity as the particles approach the corona wire; and then they are reflected back to the wall as they leave the corona wire in which the migration velocity is positive and considerably greater than the drift velocity, W_E, calculated by the classical theory. It is obvious that the particle migration velocity cannot be a single number, but it is rather a function of position because the field strength, electrostatic body force on the particle, and EHD force are position dependent.

Once the particles move into the sheltered zone or a certain EHD streamline, they are captured at the collection wall no matter how they move beyond this line. This line is called the critical EHD streamline, ψ_c. Since N_{E-C} is the parameter for how closely the particles move from the EHD streamline, ψ_j, the particle pathline starting at j, Ψ_j, is expressed as the sum of ψ_j and the distance, l_j, which is a function of N_{E-C} and number of wires. Therefore, the particle collection is described by satisfying the following equation:

$$\Psi_j = \psi_j + l_j \geq \psi_c \quad . \tag{15}$$

It is interesting to note that the particle velocity in the vicinity of the collection wall is relatively slow. Because the particle motion is slower near the wall and faster in the center, one can observe the particles rotating counterclockwise in the upper-half section and clockwise in the lower-half section. Also, a laser Doppler velocimeter (LDV) is widely used to measure the gas velocity by seeding the small particles into the ESP model. This study also provides the upper limit of particle size for employing the LDV system.

Concentration profiles for the case of $U_o = 1.22$ m/s and $2a = 5$ μm [see Figure 4(b)] are calculated, and these results are shown in Figures 5-7. Low-density monodisperse particles with uniform concentration, whose velocities are the same speed as gas flow, are assumed at the precipitator inlet.

Figure 5(a) illustrates the position-dependent concentration profiles for the two-wire precipitator. These locations are marked in Figure 4(b). By assuming that the velocity profiles are unchanged from the previous one, the concentration profiles for two, three, and six sections of the two-wire precipitator are also shown in Figure 5(b)-(d). The concentration profiles initially tend to shift to the center of the channel and reflect back toward the wall after the corona wires. There are some regions in which the concentration becomes higher than the initial value.

Figure 6 shows the concentration profiles for nonuniform inlet concentration. It appears from Figures 5 and 6 that the concentration profile is approaching the steady state beyond three two-wire precipitators, regardless of concentration profiles. This implies that the penetration becomes constant and initial concentration and velocity profiles are insignificant to the precipitator efficiency after steady state. Finer grid size may be required to obtain more accurate concentration profiles, especially near the wall and the corona-wire region where the higher concentration gradient exists.

Figure 7 shows the concentration profiles for constant $a_{i,j}$ which correspond to the plate-plate precipitator. The concentration profiles are similar to the experimental results obtained by Leonard et al. [8].

Table 1 summarizes the drift velocity obtained by the classical theory, W_E, against position-dependent migration velocity in the y direction, $\bar{V}_p$, and the fractional penetration, P_t, for the two-wire precipitator. The roles of various operating physical parameters, in terms of their influence on the collection efficiency, are established.

Leonard et al. [9] studied the particle transport for a plate-plate precipitator from the turbulent-diffusion approach. Figure 8 shows the comparison of computed penetration against Deutsch parameter, $De = W_E \cdot A/Q$ (or $N_{E-C} \cdot g$), in which the solid lines represent the results of the present study and the dashed lines represent the results obtained by Leonard et al. [9], even though they are different configurations. The penetration for the Deutsch model is obtained by using W_E and physical parameters used for this example. The effective

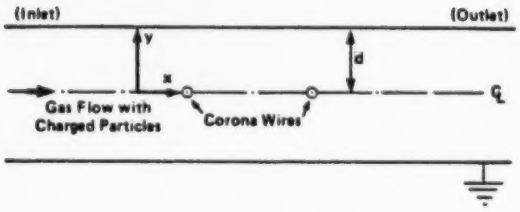

Figure 1. Physical arrangement for a mathematical model for precipitation-theory description.

The second step is the analysis of the EHD field, which is the interaction between the ionic wind and the primary gas flow. The flow is assumed to be laminar.

The third step describes the particle motion in the EHD field. The particle motion is dependent upon the EHD field and the electrostatic force on the particles.

The final step involves using the results of the third step to calculate particle concentration profile and the resulting fractional collection efficiency of the precipitator.

Since details of the theoretical analyses and experiments in the first two investigations, as well as the theoretical analysis in the third step, were previously reported [1, 4, 5], only brief descriptions are given here.

The fundamental assumptions used in this analysis are:

1. The effects of any particulate space charge are neglected.
2. Laminar flow is assumed in the EHD calculations.
3. The Reynolds number, based on corona-wire diameter, is small enough to ignore the wake behind the corona wires.
4. The effects of particle-particle interaction are neglected in the particle motion.
5. Nonideal effects such as reentrainment, sneakage, saltation effects, and back discharge are neglected.

1. Electrostatic Field and Space-Charge-Density Distribution

By using a set of reduced Maxwell's equations and current continuity equations, the two governing equations can be written as follows:

$$\nabla^2 V = -\rho_c/\varepsilon \ , \qquad (1)$$

$$\rho_c^2 = \varepsilon \nabla \rho_c \cdot \nabla V \ . \qquad (2)$$

Where: V = the potential, ρ_c = the ion-space-charge density, and ε = the dielectric constant of the air. The electric field, E, and current density, J, are related by $E = -\text{grad } V$, and $J = \rho_c bE$, where b is the ion mobility.

The boundary conditions for V in the computational domain are: $V = V_o$ measured electrical potential at the wire, $V = 0$ along the ground plate, and $\partial V/\partial n = 0$ along any symmetry line. V at the flow inlet and exit cannot be defined uniquely. The distance, however, of the boundary from the wire can be made sufficiently large (compared with the distance between the wire and the plate) so that the symmetry boundary condition may be used.

The effect of the field strength due to the uniform particle space charge was investigated. The field distribution is not appreciably affected by the space charge as long as the space charge is below 3 $\mu C/m^3$.

2. Electrohydrodynamics (EHD)

The basic equations for the two-dimensional incompressible flow of a Newtonian fluid can be simplified by using the vorticity-stream function from (ω - ψ):

$$\frac{\partial \omega}{\partial t} = -\vec{V}_f \cdot \nabla \omega + \nu \nabla^2 \omega + \nabla \times \vec{F} \ ,$$

$$\nabla^2 \psi = \omega \ ; \qquad (3)$$

where:

$$\omega = \frac{\partial u}{\partial y} - \frac{\partial v}{\partial x} \ , \quad u = \frac{\partial \psi}{\partial y} \ ,$$

$$v = -\frac{\partial \psi}{\partial x} \ , \quad \vec{F} = \rho_c \frac{\vec{E}}{\rho} \ ; \qquad (4)$$

where $\vec{V}_f$ represents the fluid velocity vector (u, v), ρ_c = space-charge density, $\vec{E}$ = field strength, ρ = gas density, and ν = kinematic viscosity.

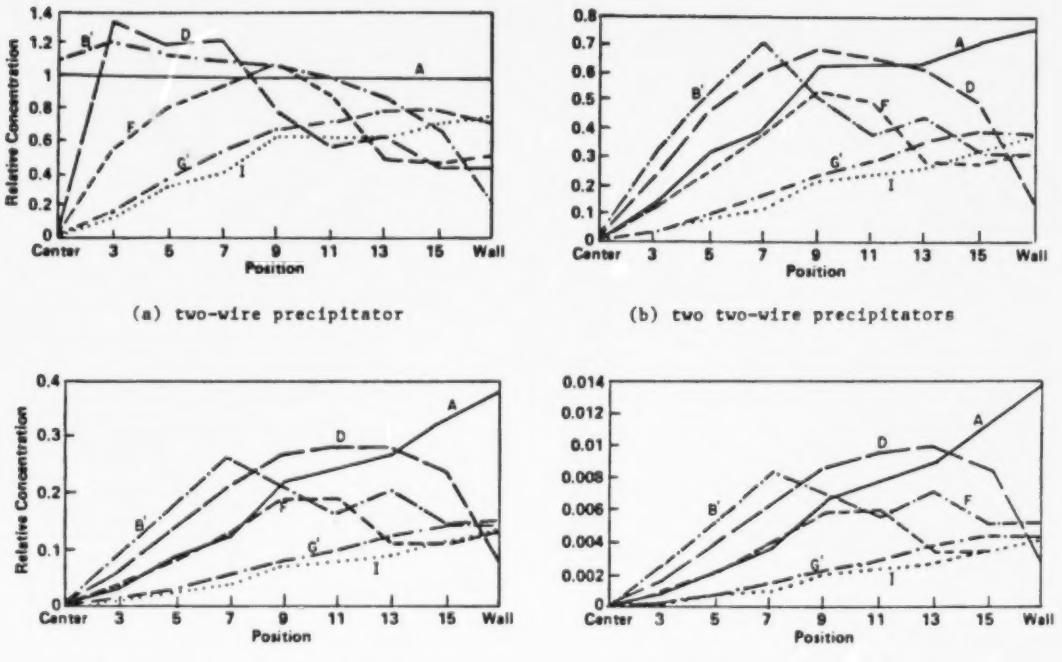

(a) two-wire precipitator

(b) two two-wire precipitators

(c) three two-wire precipitators

(d) six two-wire precipitators

Figure 5. Position-dependent concentration profiles; ———— inlet (A), —·—·— before front wire (B'), —— —— front wire (D), — — — — rear wire (F), — —·— — toward exit (G'), ... exit (I).

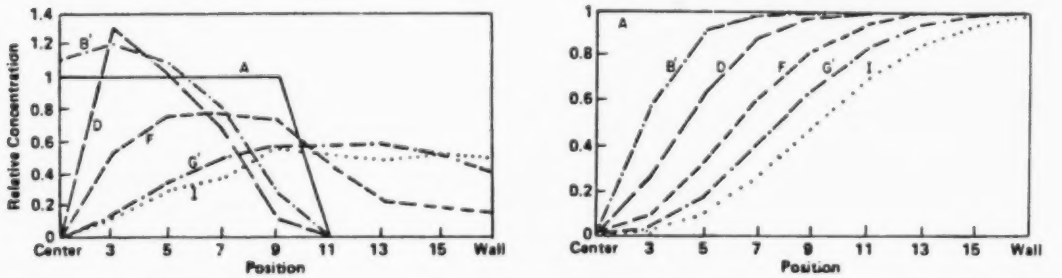

Figure 6. Concentration profiles for nonuniform inlet concentration; ———— inlet (A), —·—·— before front wire (B'), —— —— front wire (D), — — — — rear wire (F), —·—·— toward exit (G'), ... exit (I).

Figure 7. Concentration profiles for constant $\alpha_{i,i}$; ———— inlet (A), —·—·— before front wire (B'), —— —— front wire (D), — — — — rear wire (F), —·—·— toward exit (G'), ... exit (I).

TABLE 1. COMPARISON BETWEEN W_E, V_p, AND P_L

		U_o = 0.61 m/s (N_{EHD} = 2.69)				U_o = 1.22 m/s (N_{EHD} = 1.34)			
2a (μm)	W_E (m/s)	N_{E-C}	V_p (m/s) MIN	V_p (m/s) MAX	P_L	N_{E-C}	V_p (m/s) MIN	V_p (m/s) MAX	P_L
1.0	0.03	0.048	-0.25	0.33	0.88	0.024	-0.24	0.19	0.90
5.0	0.15	0.240	-0.17	0.40	0.41	0.120	-0.23	0.32	0.64

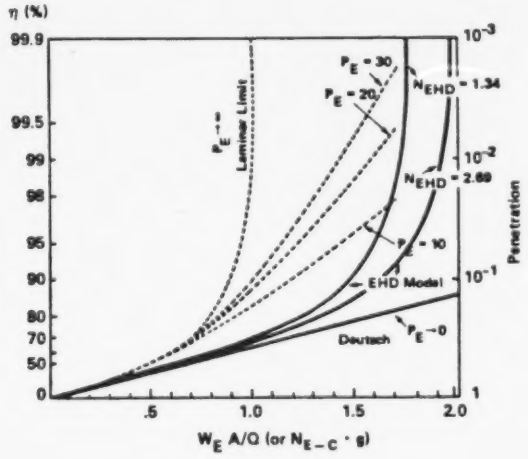

Figure 8. Comparison of computed efficiency between the wire-plate precipitator and the plate-plate precipitator.

plate length of 10.8 cm is used for this calculation. If one uses a large effective area, the Deutsch model takes less penetration.

The fractional penetration is almost identical with the Deutsch model when N_{E-C} is below 0.20 or De < 0.72, and gradually decreases as N_{E-C} increases under the present assumptions. It is quantitatively shown that increasing the secondary flow (or N_{EHD}) reduces the collection efficiency. Zero penetration is achievable for N_{E-C} > 0.48 or De > 1.73 when N_{EHD} = 1.34, even though the cell approach limits 100% efficiency, mathematically, due to numerical diffusion within the cell.

It is also clear from this figure that the penetration is considerably higher than Leonard's results for a higher Peclet number, P_E (P_E > 30), which corresponds to laminar flow. This is clearly due to the differences of the concentration profiles. Leonard showed a higher concentration profile near the wall in comparison with the present calculations for which position-dependent migration velocities are used to calculate the local concentration profiles. It is expected that the predicted efficiency based on this analysis is significantly lower than what they predicted because the net particle flux to the wall, $C_{i,j} V_p$, is much smaller.

If the concentration profile is measured and the calculated particle concentration profile is different from the experimentally determined concentration profile, the difference will be attributed to neglecting particle diffusion in a turbulent flow. The turbulent displacement of the particle can be simulated by a Gaussian random process. Therefore, the turbulent diffusivity can be derived to fit the experimentally determined particle concentration profile. As the results of this computation, the relative importance between EHD and turbulent diffusion will be determined.

If one ignores the effect of ionic wind, the EHD streamlines become more or less straight in the entire region except near the wall where the boundary layer is developing. The concentration profile becomes flatter, by which lower penetration will be achieved. Although turbulence and secondary flows are detrimental to the particle collection process, further investigations are required for the quantitative description toward a unified efficiency theory.

CONCLUSIONS

The particle motion in the EHD field is extended to include the particle concentration profiles and fractional efficiency, which allows us to look into the insight of the microscopic precipitation process. The particle motion and collection process are successfully described by

using two dimensionless parameters such as N_{EHD} and N_{E-C}. The major conclusions drawn from the present analysis are the following:

1. The EHD model predicts a reduction of collection efficiency with increased secondary flow.

2. The wire-plate precipitator predicts higher penetration compared to the plate-plate precipitator because the net particle flux near the wall is significantly smaller.

3. Good agreement is obtained between the Deutsch and EHD models for low De, but the EHD model predicts higher efficiency for higher De.

4. A steady-state concentration profile exists beyond three two-wire precipitators, regardless of inlet-concentration profiles. This implies that the penetration becomes constant and the initial concentration and velocity profiles are insignificant to the precipitator efficiency.

5. Particle collection is described by introducing the critical EHD streamline (ψ_c) and the particle streamline (ψ_i). From this perspective a new collection criterion is established.

ACKNOWLEDGMENTS

This work is partially supported by the U.S. Environmental Protection Agency (EPA) under Cooperative Agreement CR808936.

REFERENCES

[1] Yamamoto, T. "Particle Transport in the EHD Field," in Third Symposium on the Transfer and Utilization of Particulate Control Technology, Vol. II (pp. 87-96), EPA-600/9-82-0056 (NTIS No. PB83-149591), July 1982.

[2] Ushimaru, K., G.W. Butler, and P. Milovsoroff. "An Experimental and Theoretical Investigation of Electrostatic Precipitators," Flow Research Report No. 219, 1982.

[3] Shaughnessy, E.J., J.H. Davidson, and J.C. Hay. "The Fluid Dynamics of Electrostatic Precipitators: Effects of Electrode Geometry," Fifth EPA/EPRI Symposium on the Transfer and Utilization of Particulate Control Technology, Kansas City, MO, 1984.

[4] Yamamoto, T., S. Nakamura, and H.R. Velkoff. "Numerical Study of Secondary Flow Interaction in an Electrostatic Precipitator," in Innovative Numerical Analysis for the Engineering Science, University Press of Virginia, pp.3-12, 1980.

[5] Yamamoto, T., and H.R. Velkoff. "Electrohydrodynamics in an Electrostatic Precipitator," J. of Fluid Mechanics, Vol. 108, pp.1-18, 1981.

[6] Leonard, G.L., M. Mitchner, and S.A. Self. "Precipitation From Turbulent Flows," Proc. Intl. Conf. on Electrostatic Precipitation," Monterey, CA, pp.208-256, 1981.

[7] Leonard, G.L., M. Mitchner, and S.A. Self. "An Experimental Study of the Electrohydrodynamic Flow in Electrostatic Precipitators," J. of Fluid Mechanics, 127, pp.123-140, 1983.

[8] Leonard, G.L., M. Mitchner, and S.A. Self. "Experimental Study of the Effect of Turbulent Diffusion on Precipitator Efficiency," J. of Aerosol Science, 13, pp.271-284, 1982.

[9] Leonard, G.L., M. Mitchner, and S.A. Self. "Particle Transport in Electrostatic Precipitators," Atmospheric Environment, Vol. 14, No. 11, pp.1289-1299, 1980.